Determination of the effective permittivity of dielectric mixtures with the transmission line matrix method

Cédric Blanchard,[a] Jorge A. Portí,[b] Juan A. Morente, and Alfonso Salinas
Department of Applied Physics, University of Granada, E-18071 Granada, Spain

Enrique A. Navarro
Department of Applied Physics, University of Valencia, E-46980 Valencia, Spain

(Received 30 May 2007; accepted 14 July 2007; published online 17 September 2007)

In this article, the effective permittivity of two-phase dielectric mixtures is calculated by applying the transmission line matrix (TLM) method. Two slightly different TLM algorithms are considered: a hybrid approach, which combines the TLM method with a subgriding technique based on dual capacitor circuits, to allow a refined description of the material, and a standard or pure TLM approach, which uses a mesh size smaller than the typical dimension of insertions in order to appropriately describe details of the geometry. A study of the statistical distribution of permittivity for insertions in random positions is also presented, showing that the effective permittivity of the mixture tends to concentrate around the mean value as insertions reduce in size. Both TLM techniques are applied to dielectric mixtures in two-dimensional situations. When the concentration of insertions is small, the results are in close agreement with prediction formulae while for higher concentration values, deviations are observed, although basically the results fall within the range predicted by theoretical bounds. Numerical results obtained using the two TLM approaches present a similar qualitative behavior; nevertheless, a clear difference is observed between them. The study of special periodic situations with coated insertions allows us to identify the pure TLM results as more accurate than those of the hybrid approach and also explains why homogeneous distributions provide numerical values close to the theoretical limits. The effects of shape on permittivity are also modeled and deviations to the Wiener bounds are discussed in detail, using two- and three-dimensional examples in practical situations. © *2007 American Institute of Physics*. [DOI: 10.1063/1.2779216]

I. INTRODUCTION

The electromagnetic behavior and characterization of dielectric mixtures is a classical problem already addressed by Maxwell more than a century ago. This early interest has not diminished at all; on the contrary, modern artificial materials have renewed and drastically increased the attention given to this topic due to the design of challenging and sometimes previously unthinkable applications not pertinent to natural substances. High frequency applications,[1] such as perfect lens manufacture, subwavelength microwave devices, enhanced radiation by small antennas, etc., have replaced or further developed the quasistatic initial works.[2–7] In addition, the availability of powerful computers has modified the way in which these and other related problems are addressed. The earliest attempts to model dielectric mixtures concentrated on obtaining theoretical formulas to predict the effective permittivity of composite materials consisting of mixtures with several homogeneous components. Maxwell Garnett[2] (MG) considered the problem of how to find the effective permittivity ε_{eff} of a medium formed with spheres of permittivity ε_1 embedded in a host medium of permittivity ε_2, by considering only one grain of permittivity ε_1 surrounded by a medium of permittivity ε_2. The MG formula provides satisfactory permittivity values for low concentrations of insertions since the interaction with adjacent insertions is neglected. A better approximation, which solved the problem of asymmetry and the percolation threshold level, was later derived by Bruggeman,[3] who considered a spherical insertion immersed in a homogeneous medium of permittivity ε_{eff}, which has to be determined self-consistently by imposing the condition that the field inside this single grain equals the field distant from it.

Having recognized the difficulty in predicting exact values of permittivity, mainly due to the lack of information regarding the actual geometry for a given volume occupation, subsequent studies were devoted to the derivation of theoretical bounds, which limited the range of possible values. The most direct are the Wiener bounds[6] which correspond to a series or parallel connection of planar capacitors formed with both dielectric materials. Other more restrictive limits are the Hashin–Shtrikman (HS) bounds[7] which are obtained by imposing a minimum or maximum value for an energy function depending on ε_{eff}. It is worth noting that the lower HS bound corresponds to the MG prediction for the mixture under study, while the upper limit corresponds to this same model for the complementary mixture.

Due to the complexity of the problem, especially for random mixtures, numerical techniques have only been applied in recent years with the availability of powerful computers at reasonable cost. An important part of these applica-

[a]Electronic mail: cedric@ugr.es
[b]Electronic mail: jporti@ugr.es

tions starts with the derivation of an integral equation which is later numerically solved by means of different well-known methods, such as the finite element method or the method of moments.[8–11] Homogenization techniques that take into account the periodicity of the material on different scales have also been reported.[12] In a certain way, the earlier-mentioned approaches could be considered semianalytical or of an integral nature, in the sense that an important theoretical task is carried out initially to obtain an integral equation, before the specific numerical treatment is applied. These semianalytical methods provide good results, but the theoretical part requires an important reformulation if different problems or new effects are to be dealt with. Let us consider, for example, a problem devised for a static or quasistatic situation: the integral equation describing the phenomenon has nothing in common with the same problem in a high-frequency case. A different approach is provided by the so-called differential numerical methods, such as the finite differences in the time domain (FDTD) method or the transmission line matrix (TLM) method. In their basic versions, these techniques consider Maxwell equations directly, together with boundary conditions, to model a particular phenomenon numerically. Of course, solving the problem using basic equations in their most fundamental form, i.e., Maxwell and constitutive equations, may not be considered very elegant because most of the work is performed by the computer, requiring a negligible amount of prior theoretical work. The main drawback of differential methods is that the computing burden is relatively high when compared to that of semianalytical methods. In addition, there may be little modeling of detailed effects if no initial assumption is made to relieve the computer task. Nevertheless, differential numerical methods can be easily adapted to new situations merely by adding minor changes. This feature makes these methods an attractive tool for modeling dielectric materials, since, especially in random mixtures, different geometries may be solved without requiring substantial changes, a circumstance which greatly simplifies the task.

The initial applications of FDTD to modeling composite materials appeared at the end of the last century[13–15] to test the validity of mixing formulas in composite materials consisting of a host material with two-dimensional (2D) or three-dimensional (3D) spherical inclusions. The effective permittivity of a dielectric mixture is obtained by means of the reflection coefficient for a planar dielectric slab, carried out with the dielectric material surrounded by a vacuum on both sides. A statistical study comprising a high number of random distributions of spherical insertions in 2D and 3D cases provides results in the range predicted by HS bounds, except in a few cases where results are beyond the HS limits. With regard to the different prediction formulas, the results for low concentrations are quite similar because the interaction of one insertion with the remaining insertions is negligible, although a better behavior is observed for the Bruggeman formula if all concentrations are considered. The main point of these valuable FDTD works is the way in which the random geometries are considered to take into account details below a mesh size, Δl, by using dual circuits of parallel or series capacitors.

Like the FDTD method, TLM is a low-frequency numerical method which has been extensively used for the modeling of wave propagation problems, mainly of an electromagnetic nature, but also for problems in acoustics or particle diffusion.[16–20] The method is not only a numerical model for solving certain phenomena, but also a conceptual approach that does not consider the analytical equations governing the phenomenon, but deals directly with the original phenomenon by means of an equivalent transmission line circuit.[16] This conceptual nature of TLM makes this method a powerful tool which allows considering challenging problems from a hybrid numerical-conceptual point of view in an elegant and suitable way. For example, TLM has been used to model challenging situations such as radiation by thin conducting wires with a radius much smaller than the mesh size by simply including a transmission line circuit describing the inductance and capacitance introduced by the wire to the medium in which it is placed.[21] Another advantage of TLM over FDTD, especially in modeling media highly dependent on the interface position between different dielectrics, is that TLM defines all the field quantities at the same point, the center of the node, and also all the perpendicular field quantities at the interface between nodes, which simplifies the imposition of boundary conditions. In contrast, FDTD defines each component of the electromagnetic field at a different point, and even at a different time, which complicates the task of accurately defining the transition between dielectric phases. Bearing this in mind, it seems that the conceptual approach of TLM to the problem, together full definition of all the field components at the same point and time could make us think of TLM as a useful numerical tool to model situations with a high number of transitions between different phases, such as those occurring in dielectric mixtures.

In this article, the application of the TLM method for the modeling of composite mixtures is proposed. A study of 2D and 3D dielectric mixtures with the inclusion of different shapes will be considered and a comparison with prediction formulas and bounds, together with a comparison of the results obtained from combining TLM and the subgriding technique proposed by Kärkkänien *et al.*[15] will be presented, along with discussion of these results. The article is organized as follows: Sec. II is a brief description of the fundamentals of TLM; Sec. III contains a study of 2D composite materials with spherical inclusions. The study includes a convergence test, an analysis of the geometries leading to the HS bounds, and finally, the effects of size and shape. Section IV presents the results for 3D materials. Finally, the main conclusions are summarized in Sec. V.

II. FUNDAMENTALS OF TLM

The TLM method sets up a temporal and spatial calculation process which allows the temporal evolution of the electromagnetic field to be obtained. It is based on the construction of a transmission line mesh where voltage and current pulses propagate in the same way as the electric and magnetic field in the original problem.[16] The TLM mesh is formed by interconnecting unitary circuits, termed nodes. Different specific nodes can be used depending on the prob-

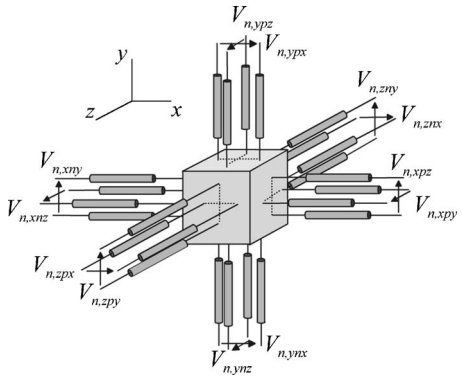

FIG. 1. Generalized 3D symmetrical condensed node.

lem under study, but independently of the geometry of the specific node, the basis of the TLM algorithm is quite simple: at time step n, a set of voltage pulses represented by the column matrix V_n^i are incident at each node in the TLM mesh, which after scattering at each node center produce a set of reflected pulses represented by the column matrix V_n^r. Both pulse sets are related by the scattering matrix of the node S by equation

$$V_n^r = SV_n^i. \tag{1}$$

Reflected pulses propagate through all the lines in the nodes and become incident pulses at neighbor nodes for the next time step. Time synchronism must be imposed when calculating the parameters of the node lines so that all voltage pulses reach the centers of the nodes at each discrete time $n\Delta t$, where Δt is the time spent by any pulse in traveling through any line from one node center to the center of the adjacent nodes.

Figure 1 shows the generalized symmetrical condensed node (GSCN) to be used in this article.[22] The node length is Δx, Δy, and Δz, along the three Cartesian directions and substitutes a cubic portion of medium of these same dimensions with electric permittivity ε, magnetic permeability μ, and electric conductivity σ. Figure 1 shows only the link lines, those which connect with the link lines of neighbor nodes and thus bear the main responsibility for propagation. In addition, stub lines, not represented in Fig. 1, are additional capacitive, inductive, or lossy lines connected only at the node centers to allow independent control of ε, μ, and σ along each Cartesian direction. The link line termed inj is i oriented, located on the negative side of the i axis, defining E_j and H_k. Link line ipj defines identical quantities on the positive side of the i axis. The capacitive and lossy lines associated with E_j are described with indexes C_j and G_j, respectively. Finally, the inductive stub associated with H_k is line L_k. All the lines are described in this manner by simply taking all the possible different values of i, j, and k in the set $\{x,y,z\}$.

Regarding the line parameters, the characteristic impedance for the inj and ipj link lines is $Z_{ij}=1/Y_{ij}$. The total voltage $V_{n,inj}$ for line inj at the nth time step consists of an incident voltage pulse $V_{n,inj}^i$ and a reflected $V_{n,inj}^r$ pulse. Similarly, pulses $V_{n,ipj}^i$ and $V_{n,ipj}^r$ correspond to the line on the positive side. The characteristic admittance of the capacitive

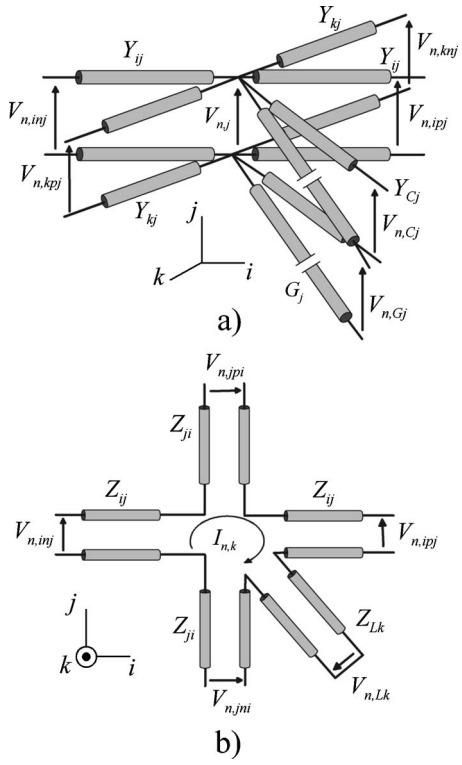

FIG. 2. (a) Parallel circuit for E_j and (b) series node for H_k.

stub associated with the j component of the electric field is Y_{Cj}, while the conductance of the resistive line is G_j. Finally, the characteristic impedance of the inductive stub associated with the k component of the magnetic field is Z_{Lk}. Pulses on these lines are denoted in a similar way to those on the link lines.

With regard to choosing the characteristic impedance or admittance of each line and the way the node defines each field component, the node can be considered as six coupled circuits: three parallel nodes to define each electric field component and three series nodes to define each magnetic field component at the node center. The tangential components at the node limits are also defined by the node, which is an interesting property when imposing boundary conditions. This circuit separation is analogous to considering the rotational Maxwell equations as six simpler scalar equations. Figure 2(a) shows the parallel circuit defining the j component of the electric field at the nth time step, $E_{n,j}$, while Fig. 2(b) is a plot of the series circuit defining the k component of the magnetic field at this same time step, $H_{n,k}$.

The circuits in Fig. 2 define a capacity and conductance associated with the j component of the electric field and an inductance associated with the k component of the magnetic field. Identifying the medium capacity, inductance, and electric conductance associated with E_j and H_k with the corresponding node capacities, inductances, and conductances provides enough equations to choose the characteristic impedance or admittance of all the lines in the node. It is worth noting that some degree of freedom is still present in this set of equations, which means that different specific nodes may be designed. In this article, the characteristic impedance of

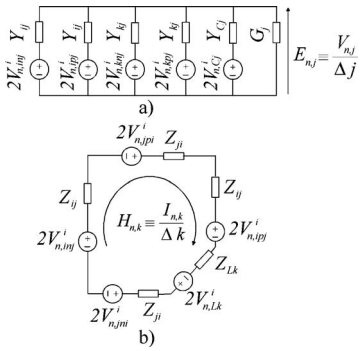

FIG. 3. Field definition of $E_{n,j}$ and $H_{n,k}$ by means of (a) the Thevenin circuit of the parallel and (b) the series node in Fig. 2.

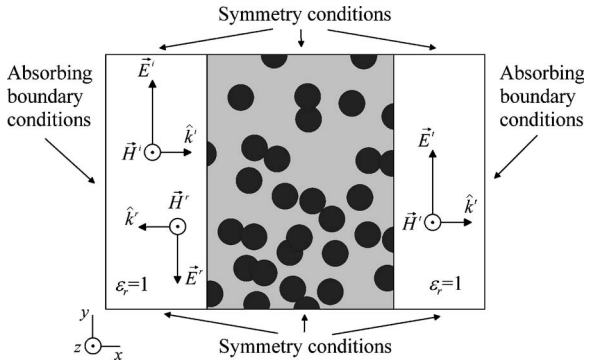

FIG. 4. Geometry of the problem.

all the link lines equals the vacuum impedance, which basically leads to the symmetrical condensed node originally proposed by Johns.[23]

Regarding the field definition at the nth time interval, the common voltage per unit length along the j direction, $V_{n,j}/\Delta j$, at the parallel circuit of Fig. 2(a) and the common current per unit length along the k direction, $I_{n,k}/\Delta k$, in the series circuit of Fig. 2(b) are analogous to $E_{n,j}$ and $H_{n,k}$, respectively. The use of the equivalent Thevenin circuits[16] for each transmission line in the circuits of Fig. 2 is a valuable tool for obtaining specific expressions of these fields exclusively in terms of the incident voltage pulses at the node. Figure 3 is a plot of the equivalent circuits corresponding to the nodes sketched in Fig. 2.

Finally, the scattering matrix may be obtained by considering unitary pulses entering the node from each line in the node. For incidence from a single link line, both a series and a parallel circuit must be considered and pulses reflected to all the lines in these circuits generated. Two of these lines appear simultaneously in both the parallel and the series circuits; these are the common lines and represent the circuit version of the coupling that exists in Maxwell equations. The remaining lines appear only in the parallel or only in the series circuits mentioned earlier; these are the uncommon lines and represent uncoupled terms for the unitary excitation under consideration. Due to this uncoupling, the pulses transmitted to the uncommon lines may be obtained directly through the transmission coefficient of the circuit. On the other hand, the partial coupling described by the existence of two common lines means that the pulse amplitude at these two lines must be obtained from charge conservation on the parallel circuit and continuity of potential on the series circuit. Detailed information concerning the TLM topics outlined in the earlier paragraphs can be found in Refs. 16 and 24.

III. EFFECTIVE PERMITTIVITY OF 2D DIELECTRIC MIXTURES

A. Preliminary topics

The effective permittivity of different two-phase dielectric mixtures consisting of different shape insertions with permittivity ε_1 embedded in a host medium of permittivity ε_2 is obtained numerically in the following sections by using a TLM mesh of GSCN with identical length Δl along the three Cartesian directions. The procedure is quite similar to that presented in Refs. 13 and 15 and sketched in Fig. 4. A dielectric slab is illuminated in the perpendicular by a plane electromagnetic wave and the TLM method is used to calculate the reflected signal numerically. This numerical reflection coefficient is compared to the theoretical reflection coefficient for a planar dielectric slab of permittivity ε_{eff}, from which this effective value can be obtained. Although the TLM results are valid for wavelengths below the dispersion limit,[25] $\Delta l < 0.1\lambda_{\min}$, where $\lambda_{\min}$ is the minimum valid wavelength in the numerical results obtained, the examples presented in this article are mostly concerned with the lowest frequency point, corresponding to a quasistatic solution, the range within which theoretical formulas and more independent information are found in the literature.

The material numerically modeled corresponds to a 2D planar slab of a dielectric mixture in which 2D spherical insertions, i.e., cylinders of infinite length, with a radius of 1 mm and relative dielectric permittivity $\varepsilon_1=18$, are randomly inserted in a host medium of relative permittivity $\varepsilon_2=2$. As swapping between insertions is allowed, the initial spherical geometry becomes even more complicated. The slab width is 20 mm, its infinite height is also modeled by using 20 mm together with symmetry conditions along the vertical direction. Finally, an arbitrary length of one TLM node along the z direction is considered together with symmetry conditions to model the 2D properties of the slab. Two vacuum regions 20 mm wide on each side of the slab are also considered. Absorbing boundary conditions at both limits of the x axis are imposed by connecting the transmission lines reaching these limits to a lumped load with the vacuum impedance.[26] This impedance matching condition is a remarkably simple boundary condition of the TLM method that produces accurate results for normally incident waves. Inclusions in the slab cause nonhomogeneities, which means that this normal incidence is not met at points near this material. However, boundaries along the x direction are chosen at sufficient distance to result in normal propagation being produced by homogenization in the vacuum region. Therefore, an appropriate abortion of unphysical reflections would be expected. This point has been tested with vacuum regions of different lengths.

Two TLM algorithms will be considered: a pure TLM and a hybrid TLM calculation. The pure TLM model uses a mesh size Δl significantly smaller than the typical dimension

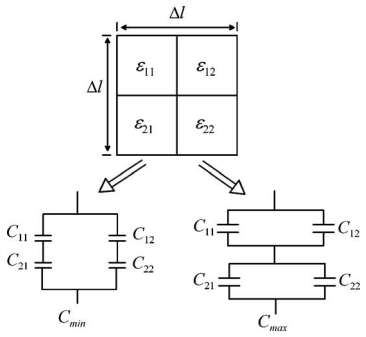

FIG. 5. Subgriding approach used to determine ε_{eff} for a large mesh size.

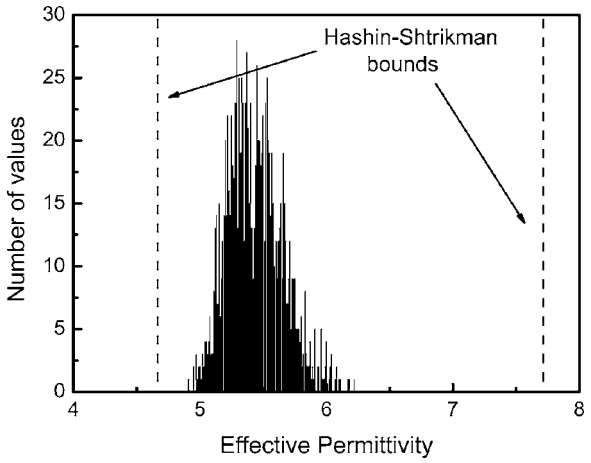

FIG. 6. Distribution of permittivity values for $p_1=0.5$ and insertion radius of 1 mm for the pure TLM model. Results compare well with a Gaussian distribution with a mean value of 5.438 and a standard deviation of 0.219.

of the inclusions. The permittivity value of each node, and therefore the admittance of the capacitive stubs, is assigned according to the permittivity of the material at the node center. In order to compare our results and also to test the validity of the subgriding technique proposed in Ref. 15 for the method FDTD, a second hybrid TLM model will also be considered, in which Δl takes much larger values comparable to the inclusion size. In this second case, details of the subnode geometry are taken into account by subdividing the main node into N parts along each direction, thus generating secondary cells of side $\Delta l/N$. This subdivision is not solved using the TLM method but allows the definition of two dual circuits of series connected or parallel connected condensers instead. Simple circuit theory concepts allows obtaining the equivalent capacity for both circuits, which provide lower and upper bounds for the capacity of the large TLM node. Finally, the effective capacity of this main node is assumed to be the average of these bounds, from which it is easy to obtain the effective permittivity of an equivalent condenser. Figure 5 shows both dual circuits in a 2D case for $N=2$. As pointed out earlier, these two auxiliary condenser circuits are not solved in detail by using the TLM method, but taking into account simple circuit theory concepts to define a global permittivity for the large node, which is then solved by means of the TLM method. The idea is to define a hybrid technique which combines the advantages of using large values of Δl for the main TLM node, i.e., less memory and computing time required, but at the same time to describe the geometry in more detail by using simple circuit theory to support the TLM solution. As already noted in Ref. 15, the approach is expected to work properly when interfaces between different materials are vertical or horizontal, while arbitrary geometries, such as those presented by spheres or ellipses, are only approximately described.

B. Convergence, size effect, and statistical distribution of results

Let us initially concentrate on the distribution of results for the different geometries possible for a given concentration. A total of 1000 different geometries for $p_1=0.5$ were modeled using both TLM techniques. The node size is 0.1 mm for the pure TLM results and 1 mm for the hybrid solution with auxiliary subdivisions of 0.025 mm, i.e., with $N=40$. Details regarding these lengths are discussed later in this section. In each case considered, insertions of 1 mm radius were randomly located in the slab until the desired volume concentration was obtained. Of course, a variation in the specific location of the insertions means that the effective permittivity obtained is also variable. Figure 6 is a plot of the number of geometries providing each effective permittivity value in the set of random geometries considered. In effect, the results show a statistical distribution around a mean value which resembles a Gaussian distribution with a mean value of 5.438 and a standard deviation of 0.219. Results are similar for the hybrid TLM method, even with identical standard deviation, but with a different mean value of 5.715.

In this situation and to test the effect of insertion size, a similar test was performed for insertions with a larger radius of 2 mm. The distribution of effective permittivity is quite similar, but now with a mean value of 5.231 and a greater standard deviation, 0.406. The Gaussian shape is slightly distorted, but the most remarkable facts are that the distribution is wider, even the HS bounds have been surpassed in a nonnegligible number of geometries. This concentration of permittivity for small insertions may be explained by the fact that a smaller size means that a higher number of insertions is needed to reach a certain concentration. Therefore, if the position of a given particle is randomly changed to another position in another random distribution, the fact that there are still a high number of small insertions to be allocated means that it is relatively likely that another particle may take the position occupied by the earlier-mentioned particle in the previous geometry. In other words, smaller insertions increase the similarity between the different geometries and thus the effective permittivity of the mixture is more concentrated around its mean value. It is worth noting that this concentration effect is of great interest for the design and practical manufacturing of composite dielectrics since the natural uncertainty due to possible differences in the internal structure is minimized.

The convergence test to determine the appropriate Δl is performed for three particular geometries providing ε_{eff} close to the mean, maximum, and minimum values for this concentration. The tests use TLM nodes with $\Delta x=\Delta y=\Delta z=\Delta l$, together with a reference mesh size of $\Delta l_{\text{ref}}=1$ mm. Finer

TABLE I. Numerical effective permittivity for three different distributions obtained by using the hybrid TLM method with $\Delta l=1$ mm and the pure TLM method with $\Delta l=1$ mm/N. Distributions 1, 2, and 3 correspond to geometries around the low, average, and maximum permittivity values for $p_1=0.5$.

Distribution modeled/numerical method	$N=10$	$N=20$	$N=40$	$N=80$
Low epsilon distribution/hybrid TLM	5.134	5.133	5.145	5.147
Low epsilon distribution/pure TLM	4.915	4.881	4.865	4.860
Medium epsilon distribution/hybrid TLM	5.524	5.509	5.506	5.504
Medium epsilon distribution/pure TLM	5.289	5.257	5.247	5.243
High epsilon distribution/hybrid TLM	6.416	6.425	6.428	6.429
High epsilon distribution/pure TLM	6.220	6.152	6.143	6.138

detail is achieved in the pure TLM solution by considering smaller nodes of length $\Delta l=\Delta l_{\text{ref}}/N$. Increasing the subdivision parameter N produces higher memory requirements due to an increase in the number of nodes in the mesh, but also due to a reduction in the maximum allowable time step, $\Delta t=\Delta l/(2c)$, where c stands for the vacuum speed of light. With the hybrid TLM method, the parameter N is only an auxiliary subdivision parameter, which splits Δl_{ref} into N parts along each direction to define two dual circuits, like those presented in Fig. 5, corresponding to upper and lower bounds for the permittivity of the node. Nevertheless, it is worth noting that for any value of N, the TLM mesh size and the time step are kept at a constant value, $\Delta l=\Delta l_{\text{ref}}$ and $\Delta t=\Delta l_{\text{ref}}/2c$, respectively. Table I shows the effective permittivity obtained for different values of N in the two cases. It can be seen that results obtained with the hybrid technique require a higher value of N, around 80, to reach an acceptable convergent result, although the numerical burden is not significantly increased because the mesh size is always maintained at 1 mm. With the pure TLM technique, results tend to reach a convergent value for lower values of N around 20 or 40. Higher values of N provide almost identical results but the increase in memory storage and computing time required is considerable and unnecessary.

Once the appropriate N parameter is determined, the effective permittivity is obtained in the whole range of p_1 for a dielectric mixture with $\varepsilon_1=18$ and $\varepsilon_2=2$ using both methods. Numerical values obtained using the pure TLM method with $N=20$ and the hybrid method with $N=80$ are shown in Fig. 7. The two results are qualitatively similar, always located within the Wiener bounds and in most cases between the HS bounds, but a clear difference is observed between the pure and the hybrid TLM results. With regard to prediction formulas, the Bruggeman model predicts more accurately than the MG formula (lower HS bound), but theoretical predictions become poorer as p_1 increases. The difference between the hybrid and the pure TLM results is already observed in Table I. Figure 8 shows that similar a behavior and deviation are observed for the inverted mixture with $\varepsilon_1=2$ and $\varepsilon_2=18$ for the hybrid and pure TLM results. A difference between numerical results and theoretical formulas is to be expected, but the difference between numerical results for pure and hybrid TLM is more annoying since the problem is not one of convergence. The question is which of these numerical results is more accurate? It would appear that the pure

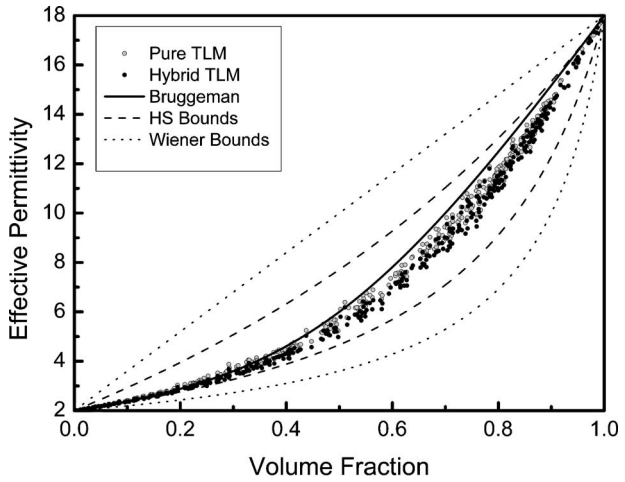

FIG. 7. Effective permittivity vs volume fraction of insertions for a random mixture with $\varepsilon_1=18$ and $\varepsilon_2=2$ obtained with the pure and the hybrid TLM methods.

TLM solution should provide the best results because the details are considered directly without averaging approaches of auxiliary circuits, but since an experimental test is impossible, an appropriate numerical test must be carried out.

C. Numerical validation using Hashin–Shtrikman bounds

So far, we have verified that statistically different geometries present permittivities within the range predicted by the Wiener bounds, most of them also in the range of the HS bounds. These latter limits have been claimed to be the most restrictive ones if only the host and insertion permittivities and concentration are determined; in other words, most limiting bounds would require additional information such as the shape, size, and specific spatial distribution of the insertions. At this point, one wonders if these bounds can be attained by a specific geometry. It can be shown[7] that one of the HS bounds corresponds to a material in which spheres of one phase are coated with a spherical shell of the other phase. The ratio between the two phases of the coated sphere must equal the ratio of the composite volume fractions,

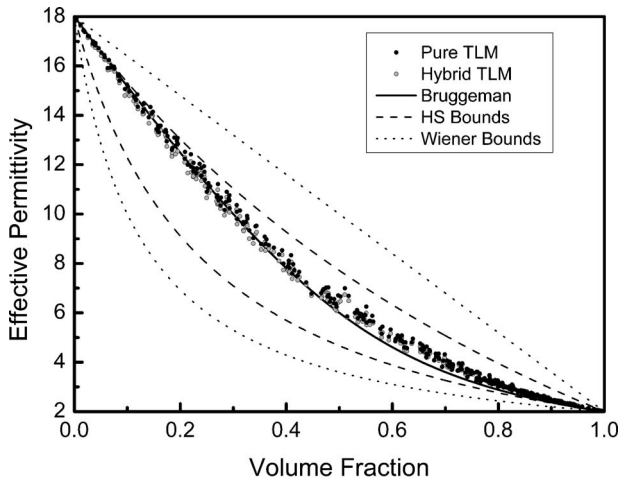

FIG. 8. Effective permittivity vs volume fraction of a random mixture with $\varepsilon_1=2$ and $\varepsilon_2=18$ obtained with the pure and the hybrid TLM methods.

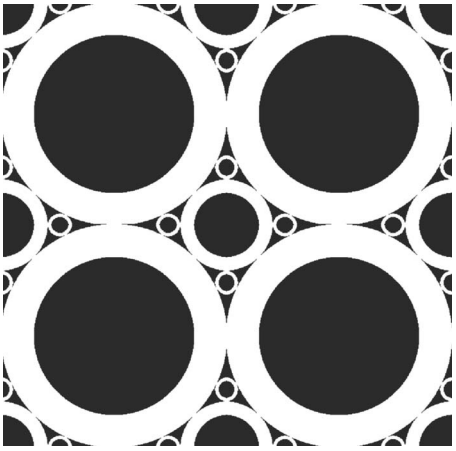

FIG. 9. Periodic structure with effective permittivity of a Hashin–Shtrikman bound. Each sphere core is phase 1 and the coating is phase 2.

p_1/p_2. Once the coated spheres have been arranged in such a way that they occupy a maximum of the available volume, i.e., they are in contact with neighbor spheres, identical but smaller structures must be placed in the remaining free space. This periodic assemblage is repeated an infinite number of times until the whole space is filled. Of course, this process is impossible to model in practice since we cannot fill the entire slab with circles. However, we can approach the ideal configuration with three levels of insertions, as is suggested in Fig. 9. Let us assume that phase 1 is the core of the insertion and that phase 2 is the coating. It is worth noting that the case $\varepsilon_1 > \varepsilon_2$ represents the lower HS bound, while the dual case, $\varepsilon_2 > \varepsilon_1$, yields the upper HS bound.

Our test consists in calculating the reflection coefficient for a dielectric slab whose internal geometry is that of Fig. 9 with both TLM methods. The slab width is again 20 mm and three levels of coated spheres are considered. Unless a very thin grid is used, the addition of a fourth size of smaller coated spheres would have only a limited effect. The radius of the largest spheres is 1 mm, so a total of ten large spheres are considered along the horizontal direction. As regards the vertical direction, only one largest sphere is used together with appropriate symmetry conditions to take into account infinite height of the slab. The mesh size used for the pure TLM calculations is $\Delta l = 0.05$ mm, which means that the dielectric slab size is 400×40 in TLM node units. As regards the hybrid TLM method, the node size is $\Delta l = 1$ mm, so the dielectric slab size is 20×2 in TLM node units, but 60×60 auxiliary subdivisions are used for each node in order to estimate the permittivity of the node through the capacitor circuits shown in Fig. 5. Pure and hybrid TLM results for the two dual mixtures are shown in Fig. 10 in terms of the volume fraction $p_{\max}$ of the phase with higher individual permittivity. The lower branch in each TLM model corresponds to $\varepsilon_1 = 18$, $\varepsilon_2 = 2$, and $p_{\max} = p_1$, while the upper one corresponds to a dual situation with inverted permittivities in which $p_{\max} = p_2$. As expected, the pure TLM results are in close agreement with the theoretical HS bounds, while the hybrid TLM approach is unable to accurately reproduce the behavior of this challenging geometry. This result enables us to identify the pure TLM technique as a more accurate solution than the hybrid one and therefore the following mixtures will be modeled only with this technique.

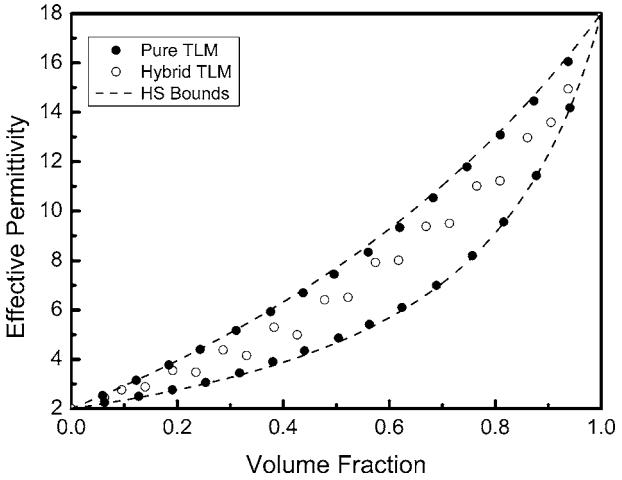

FIG. 10. Effective permittivity vs volume fraction, $p_{\max}$, of the phase with higher permittivity in the geometry of Fig. 9. The lower branches model $\varepsilon_1 = 18$ and $\varepsilon_2 = 2$, while the upper branches correspond to the dual mixture. The radius of the largest spheres is 1 mm, the node length is 0.05 mm for the pure TLM solution and 1 mm for the hybrid TLM solution.

D. Effect of inclusion shape on effective permittivity

Let us now consider several types of inclusion with different shapes. The geometries of the inclusions studied are: circles, squares, and ellipses with different eccentricities. For simplicity's sake, inclusions, again with relative permittivity $\varepsilon_1 = 18$, are now periodically placed in a host medium whose permittivity is $\varepsilon_2 = 2$. The number and position of the inclusions is fixed but their section is variable, which permits the study of effective permittivity in terms of the inclusions volume fraction. Permittivity results for the pure TLM model are shown in Fig. 11. The Wiener and HS bounds are also included, together with the Bruggeman formula. Let us also note that the lower HS bound corresponds to the MG prediction formula.

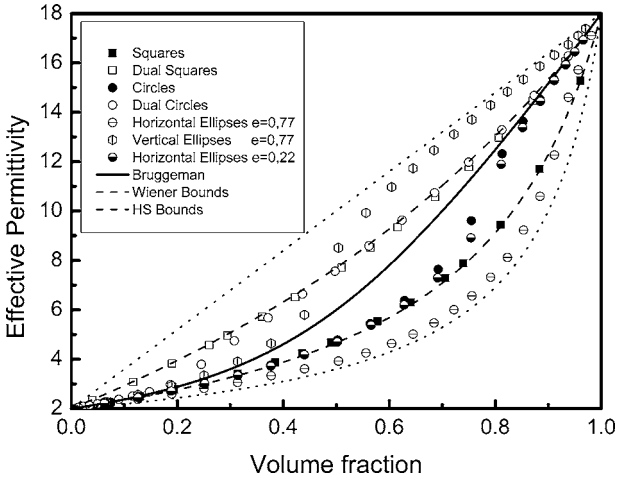

FIG. 11. Effective permittivity obtained with the pure TLM model vs concentration for a homogeneous distribution of 2D inclusions with different shapes.

As might be expected for low concentrations and irrespective of the type of inclusions, results are in close agreement with the MG, i.e., the lower HS bound and the Bruggeman prediction formulas, while a deviation is observed in the case of increased concentration due to interaction between neighbor insertions. This deviation, which may be more or less important, depends on the form of the inclusion. It is worth noting that the shape effect is accentuated at certain concentrations because a concentration-dependent swapping exists between inclusions when the concentration is large enough. In the case of ellipses of high eccentricity, 0.77, this swapping happens at $p_1=0.504$ and a further increase in concentration causes the mixture to approach the vertical or horizontal planar capacitor geometries. These planar geometries are the ones used to define the Wiener bounds, which explains the sudden changes toward these limits observed in ε_{eff} for both orientations. For example, an increase in ε_{eff} is observed in Fig. 11 for vertical ellipses around $p_1=0.5$, which now resembles a vertical and planar distribution of a two-phase dielectric mixture corresponding to the upper Wiener limit. This change in ε_{eff} perfectly fits the swapping concentration mentioned earlier. The case of horizontal ellipses is similar, but results now approach the lower Wiener bound because the system now tends to a horizontal and planar distribution of a two-phase dielectric mixture. This change in the overlapping region is also observed for cylinders and ellipses with a small eccentricity of 0.22, although an explanation of the results is less obvious.

A special case, shown in Fig. 11, is that exhibited by cubic inclusions, which follow the lower HS bound, i.e., the MG formula, almost exactly. This behavior has already been detected in other works and has been qualified as surprising.[9,12] Effectively, due to the homogeneous allocation of insertions, it would be reasonable to expect a dielectric constant around the mean value for that concentration rather than a value close to the lower bound. However, maybe this is not so surprising if we think of this homogeneous distribution in terms of the theory giving rise to the HS bounds. In effect, as mentioned in Sec. III C, the geometry of Fig. 9, consisting of spherical coated insertions arranged at intervals to fill the whole space, leads to a maximum or minimum value of ε_{eff}. The spherical shape means that an infinite number of progressively smaller coated spheres will be positioned to fill the whole space not covered by previous larger spheres. But if we substitute square coated cylinders for the larger coated circular cylinders, only one level of coated insertions would fill the whole space and no more smaller square cylinders would be required. This means that the homogeneous mixture consisting of cubic insertions is not as different as it seems from the periodic geometry of Fig. 9, which could explain why the results are close to the lower HS bound, i.e., to the MG formula. It is worth noting that we have also modeled a dual mixture in which square cylinder insertions with $\varepsilon_1=2$ are homogeneously distributed in a host medium with permittivity $\varepsilon_2=18$, labeled dual squares in Fig. 11. As expected, the effective permittivity corresponds almost exactly to the upper HS bound.

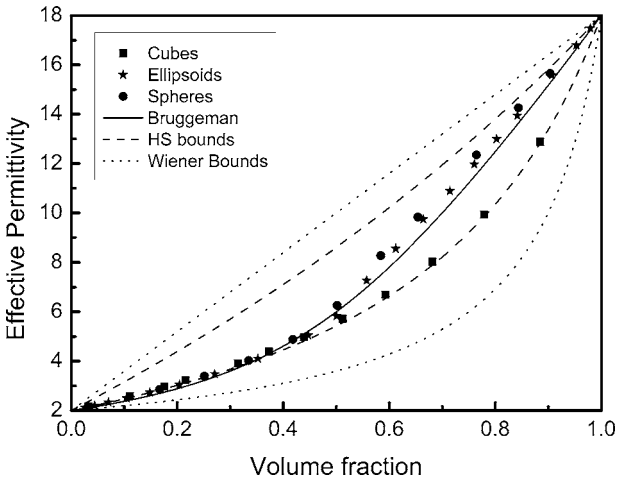

FIG. 12. Effective permittivity obtained with the pure TLM model vs concentration for a homogeneous distribution of 3D inclusions with different shapes.

IV. EFFECTIVE PERMITTIVITY OF HOMOGENEOUS 3D TWO-PHASE DIELECTRIC MIXTURES

Finally and for completeness' sake, results for 3D mixtures are shown in Fig. 12. The node size is $\Delta l=0.1$ mm along the three Cartesian directions in all cases. The typical dimensions of insertions vary but are close to 1.7 mm for the most unfavorable case considered, in which p_1 is around 0.1. All the insertions are uniformly distributed, so symmetry conditions are imposed to model only one quarter of each insertion, thus reducing memory and calculation time requirements. The results are qualitatively similar to those for 2D situations but swapping now happens at lower concentration values and deviations to the HS limits are observed earlier.

V. CONCLUSION

In this article, the TLM numerical method was applied to obtain the effective permittivity of dielectric mixtures with inclusions of different shapes and sizes. Two TLM numerical approaches were considered: a hybrid TLM technique which, by means of an auxiliary subgriding technique based on a pair of dual capacitor circuits, allowed the use of a mesh size comparable to the inclusion dimensions, and a pure TLM approach in which finer detail was achieved by using a mesh size smaller than the typical dimension of insertions. Both techniques were tested with two-phase dielectric mixtures, providing results in good agreement with predicting formulas when insertion concentrations were small but an expected deviation for larger concentrations was observed, due to interaction between neighbor insertions. In this high concentration range, results were mostly within the limits predicted by the restrictive HS bounds. Although the results obtained with the two TLM techniques showed a qualitatively similar behavior, we detected an important difference between them. The study of the special periodic geometries of coated insertions enabled us to identify the pure TLM results as more accurate than those of the hybrid TLM. In addition, these coated insertions offered an explanation as to why some homogeneous distributions of insertions may provide effective

permittivities closer to the HS bounds than to the mean permittivity value for that concentration. The effects of insertion size and shape were also considered. With regard to size inclusion, smaller insertions produced a lower dependence of the effective permittivity on the specific geometry, which seems to relate to the high number of inclusions required for a given concentration. This size effect reduces the statistical importance of the variations in the specific location of each insertion concentrating the permittivity values around the mean value. This may be of interest for the design of dielectric mixtures with a well defined permittivity value, despite the uncertainty concerning the internal structure of the material. Finally, with reference to the shape effect, a deviation toward the Wiener bounds was observed when changes veered toward a vertically or horizontally planar distribution of the dielectrics constituting the mixture, this effect being more accentuated once the swapping between neighbor insertions occurred.

ACKNOWLEDGMENTS

This work has been supported in part by the "Ministerio de Educación y Ciencia"of Spain under Project Reference No. FIS2004-03273 cofinanced with FEDER funds of the European Union. The authors would also like to thank A. Espinosa for her help in preparing the manuscript.

[1]N. Engheta and R. W. Ziolkowski, *Metamaterials. Physics and Engineering Explorations* (IEEE, Piscataway, NJ, 2006).
[2]J. C. M. Garnett, Philos. Trans. R. Soc. London, Ser. A **203**, 385 (1904).
[3]D. A. G. Bruggeman, Ann. Phys. **416**, 636 (1935).
[4]R. Landauer, in *Conference Proceedings on Electrical Transport and Optical Properties of Inhomogeneous Media*, edited by J.C. Garland and D.B. Tanner (American Institute of Physics, New York, 1978), p. 2.
[5]D. J. Bergman, Phys. Rep. **43**, 377 (1978).
[6]O. Wiener, J. Math. Phys. **62**, 256 (1910).
[7]Z. Hashin and S. Shtrikman, J. Appl. Phys. **33**, 3125 (1962).
[8]B. Sareni, L. Krähenbühl, A. Beroual, and A. Nicolas, IEEE Trans. Magn. **33**, 1580 (1997).
[9]K. W. Whites and F. Wu, IEEE Trans. Magn. **50**, 1723 (2002).
[10]B. Sareni, L. Krähenbühl, and A. Beroual, J. Appl. Phys. **81**, 2375 (1997).
[11]F. Wu and K. W. Whites, IEEE Trans. Antennas Propag. **49**, 1174 (2001).
[12]O. Ouchetto, C. Qiu, S. Zouhdi, L. Li, and A. Razek, IEEE Trans. Microwave Theory Tech. **54**, 3893 (2006).
[13]O. Pekonen, K. Kärkkäinen, A. H. Sihvola, and K. I. Nikoskinen, J. Electromagn. Waves Appl. **13**, 67 (1999).
[14]K. Kärkkäinen, A. H. Sihvola, and K. I. Nikoskinen, IEEE Trans. Geosci. Remote Sens. **38**, 1303 (2000).
[15]K. Kärkkäinen, A. H. Sihvola, and K. I. Nikoskinen, IEEE Trans. Geosci. Remote Sens. **39**, 1013 (2001).
[16]C. Christopoulos, *The Transmission-Line Modeling Method: TLM* (IEEE, New York, 1995).
[17]J. A. Portí, J. A. Morente, H. Magan, and D. P. Ruiz, IEEE Trans. Antennas Propag. **46**, 741 (1998).
[18]D. De Coogan, *Transmission Line Matrix (TLM) Techniques for Diffusion Applications* (Gordon and Breach Science, Amsterdam, 1998).
[19]W. O'Connor and F. Cavanagh, Appl. Acoust. **50**, 247 (1997).
[20]J. A. Portí and J. A. Morente, J. Sound Vib. **241**, 207 (2001).
[21]P. Naylor and C. Christopoulos, IEEE Trans. Microwave Theory Tech. **38**, 328 (1990).
[22]V. Trenkic, C. Christopoulos, and T. M. Benson, IEEE Trans. Microwave Theory Tech. **44**, 2129 (1996).
[23]P. B. Johns, IEEE Trans. Microwave Theory Tech. **35**, 370 (1987).
[24]J. A. Portí, J. A. Morente, and M. C. Carrión, Electron. Lett. **34**, 1763 (1998).
[25]J. A. Morente, G. Jiménez, J. A. Portí, and M. Khalladi, IEEE Trans. Microwave Theory Tech. **43**, 452 (1995).
[26]J. A. Morente, J. A. Portí, and M. Khalladi, IEEE Trans. Microwave Theory Tech. **40**, 2095 (1992).